RF Sensor Networks for Device-Free Localization: Measurements, Models and Algorithms

Neal Patwari and Joey Wilson

***Abstract*—We discuss the emerging application of device-free localization using wireless sensor networks, which find people and objects in the environment in which the network is deployed, even in buildings and through walls. These networks are termed "RF sensor networks" because the wireless network itself is the sensor, using RF signals to probe the deployment area. Device-free localization in cluttered multipath environments has been shown to be feasible, and in fact benefits from rich multipath channels. We describe modalities of measurements made by RF sensors, the statistical models which relate a person's position to channel measurements, and describe research progress in this area.**

I. Introduction

Wireless networks are ubiquitous. Wherever we are, we are interacting with radio frequency (RF) electromagnetic (EM) waves. In this article, we review efforts to use the changes caused by people's interaction with the RF EM wave field to infer their position. We call the static wireless devices used for this purpose "RF sensors", because they are used to measure the signal on each link between devices. Such a network we call a *RF sensor network*, as opposed to the term "wireless sensor network", which refers to a general-purpose network of sensors. This area of research is also called "device-free" localization (DFL) [1] to emphasize that a person[1] does not need to be carrying a wireless device to be detected and located, or "sensorless sensing" because sensor network researchers typically do not consider the radio to be a sensor [2]. With or without a radio transmitter (TX) or receiver (RX) on them, a person's presence at a location impacts the radio waves nearby. This area is related to radar, including ultra wideband (UWB) and multiple-input multiple-output (MIMO) radar systems, but is not limited to these frameworks.

There is an advantage to sensing RF energy as opposed to light, infrared, or thermal energy when attempting to infer people's movements. Visible light cameras largely depend on daylight; light and infrared do not penetrate smoke. Radio frequency waves can penetrate non-metal walls and smoke [3], unlike light, thermal, or mm-wave energy. Thus RF-based DFL is a complementary security technology which does not require floodlights to work at night, and can locate people in a smoke-filled building, or from the exterior of the building. Other radio-based localization technologies exist, sometimes labeled as real-time location systems (RTLS), which require each person or object to be attached to a radio transmitter tag, which is then located based on the signals received from that tag at multiple other sensors [4]. However, in security or emergency applications, one cannot expect all people of interest to be wearing a radio tag.

With these advantages, DFL has several applications. DFL technologies may complement existing localization systems which use tags to locate and identify people by combining RF sensor measurements from two sources: (1) from signals received from the transmitter tag, and (2) measurements between the static RF sensors. As such, DFL may improve existing RTLS systems. As another example, DFL techniques may be useful for police or emergency responders approaching a dangerous building. Prior to entering, they may wish to deploy a RF sensor network around the building, either independently from, or in concert with, an existing wireless network in the building. Then, they can use DFL techniques to locate and track people moving within the building. As another example, RF sensor networks may be deployed within large buildings and facilities, as an alternative to more invasive video camera networks, in order to ensure compliance with safety and security rules. These networks may work in concert with context-aware computing and control systems to prevent accidents, and protect confidential information.

An RF sensor network effectively measures many sections of the environment because many links between pairs of radios exist in an area, and each link measures a different section of space. Thus the word *tomography*, defined as imaging by sections, applies to estimation in RF sensor networks. However, RF radio wave propagation is not solely by line-of-sight (LOS) propagation [5]. In fact, we typically expect the power in non-line-of-sight (NLOS) paths to dominate, except in unobstructed short-range links [6]. Thus computed tomography (CT) techniques developed for x-ray scanners, which assume that each measurement is along a straight line through the medium [7], do not directly apply – we cannot simply scale up the size of an area, scale down the frequency of emission, and achieve proportional results.

Yet, as we describe in this article, a significant quantity of research has shown results that locate people in buildings using RF sensor measurements [2], [8], [9], [1], [10], [11], [12], [13], [14], [15], [16], [17]. Results have been presented which count the number of people moving [9], estimate a person's location [18], [13], [17], [14], and image the movements in an area of interest [11], [12], [13], [15], all in real-world multipath environments. Both location estimation (estimating a person's coordinate at one time) and tracking (estimating a person's

N. Patwari and J. Wilson are with the Department of Electrical and Computer Engineering, University of Utah, Salt Lake City, USA. This material is based upon work supported by the National Science Foundation under Grant No. #0748206. E-mails: npatwari@ece.utah.edu, and joey@xandem.com.

[1]In this paper, we use "person" to refer generically either to a person or a mobile object.

velocity and sequence of positions over a duration of time) have been reported, with accuracy of less than one meter of average error [8], [14], [13] or less than two meters median error over a 1500 m^2 area [17]; these results are at least as good as reported location error when locating radio tagged objects [4], [19], so the accuracy is surprising.

How are these systems able to counteract the effects of multipath in an effort to track movement? The answer to this question is that successful DFL systems have been designed to take advantage of the effects of multipath propagation, rather than try to counteract them. Multipath fading becomes the signal, not the noise. We show in this review article how multipath fading is used for the benefit of DFL systems. We present the results of the growing literature for DFL in three parts, first discussing the RF sensor measurement modalities in Section II, then presenting models for the measurements in Section III, and then presenting the algorithms and results in Section IV. Finally, we conclude in Section VI.

II. Measurements

Device-free localization (DFL) employs networks which measure properties of the radio channel between many pairs of RF sensors. Changes in channel properties provide information about the position of objects in the environment. *What types of radio channel measurements are most appropriate for DFL?* In this section, we introduce several modalities of measurements of radio channel characteristics which can be used to infer the location of people and objects in a building. We discuss the advantages, and disadvantages of these modalities.

A. Ultra-Wideband (UWB)

First, we discuss the use of UWB measurements for purposes of DFL. Ultra-wideband receivers measure the amplitudes, time delays, and phases of the multipath signals which exist in the radio channel. Measured at multiple probing times t, UWB measurements and the changes between them can be used to infer both the properties of the static propagation environment, and the changes in the environment which might indicate a moving person or object. UWB transceivers are certainly more cost-prohibitive than narrowband transceivers, but the ability to distinguish time delay is a key benefit.

Transmitting and receiving an UWB pulse (or for that matter, high bandwidth signal) allows one to measure the channel impulse response (CIR). Assume at time t, $N(t)$ multipath components arrive at the RX, with the ith component having complex amplitude gain of $\alpha_i(t)$ and time delay $\tau_i(t)$. As a complex value, $\alpha_i(t)$ can be written as $|\alpha_i(t)| \exp[j\angle\alpha_i(t)]$. The CIR is [5],

$$h(t,\tau) = \sum_{i=1}^{N} \alpha_i(t)\delta(\tau - \tau_i(t)) \tag{1}$$

where $\delta(\cdot)$ is the Dirac impulse function.

The knowledge of time delay provides important information about position. Comparing the delay $\tau_i(t)$ to the line-of-sight time delay (assuming it is known) indicates the excess delay, which gives some knowledge of the spatial incidence of the ith multipath. For example, if the path was assumed to result from a single "bounce", *i.e.*, change in direction, then that object that caused the bounce is located somewhere on an ellipse of a certain size, with the TX and RX as foci [20]. When time delay is measured on multiple links, the intersection between ellipses is an estimate of the object location.

B. Narrowband

Next, we discuss narrowband channel measurements for purposes of DFL. Narrowband receivers cannot provide information about individual multipath, only the signal magnitude and phase as a whole. However, narrowband transceivers are produced in high quantity for commercial applications, thus their low cost is a key part of enabling large scale RF sensor networks.

Narrowband wireless devices simply measure the sum of the contributions of all multipath. We consider a continuous-wave (CW) signal, which results in a received complex baseband voltage, $\tilde{V}$, of

$$\tilde{V} = V_T \sum_{i=1}^{N} \alpha_i(t) = \sum_{i=1}^{N} V_i(t) \tag{2}$$

where V_T is the complex baseband voltage at the TX, and $V_i(t) = V_T\alpha_i(t)$ is the complex baseband voltage of component i at the RX [5].

There is information about position contained in $\tilde{V}$. First, the information in the magnitude of $\tilde{V}$ will be discussed below. Secondly, $\tilde{V}$, when compared to the $\tilde{V}$ measured at other RX locations or at multiple antennas, provides information about the azimuth or elevation angles-of-arrival of the multipath signals [21], and can be used in multiple wave field reconstruction techniques as discussed in Section IV-B.

Typical distributed wireless sensors have difficulty with accurate timing synchronization [22], and for coherent phase measurements, phase synchronization is required. Phase synchronization means that the carrier used by two different transceivers must have the same phase. Since the carrier phase changes from 0 to 2π each carrier cycle, timing synchronization errors must be much less than $1/f_c$, where f_c is the carrier frequency. For example, at 900 MHz, timing errors must be much smaller than one nanosecond. A future challenge in DFL is to either provide practical means for phase-coherent measurements of $\tilde{V}$ at disparate sensors, such as interferometric methods [23], or to achieve some of the benefits of phase-coherent measurements using non-coherent measurements.

C. Received Signal Strength (RSS)

In this section, we consider measurements of RSS for purposes of DFL. Compared to the narrowband measurements presented above, RSS is a magnitude-only measurement. Measurements of RSS are ubiquitous in nearly all wireless devices. The received power is the squared magnitude of the complex baseband voltage $\tilde{V}$. What we typically call the "received

signal strength" (RSS) is a measurement of the received power in decibel terms. For a narrowband receiver, this power is

$$R_{dB} = 20\log_{10}|\tilde{V}| = P_T + 20\log_{10}\left|\sum_{i=1}^{N}\alpha_i(t)\right| \quad (3)$$

where $P_T = 20\log_{10}|V_T|$.

One source of information in R_{dB} is its magnitude. For links with a strong LOS component, when that strong component is blocked, R_{dB} tends to decrease. This is called shadowing, and a sharp decrease in R_{dB} can be used to infer that a person or object is located along the LOS path [11].

Further, multipath fading is a source of location information. Depending on the phases of each $V_i(t)$, the sum in (2) may be destructive (with opposite phases) or constructive (with similar phases). Measurements of fading are one source of information about the location or number of moving people in the environment, as discussed in Section IV. Fading can be quantified, for example, with the variance of R_{dB} [13], [9], by the absolute value of differences [8], [24], or even the link quality indicator (LQI) [9].

The variance of R_{dB} has been shown to be approximately linearly related to the total power in multipath components affected by the movement in the environment [25]. We will discuss what is meant by "affected" and provide models for the effect in Section III-D.

Although individual RSS measurements are less informative about person location than UWB measurements, for example, the low cost of RSS-only narrowband radios will allow more nodes for a given price. Since measurements are made between pairs of RF sensors, the number of measurements increases as $\mathcal{O}\left(N^2\right)$, and the overall capability of the RF sensor network can be very significant.

D. Polarization

Finally, we consider the DFL information contained in the polarization of the EM wave at the RX. The polarization is useful to detect movement in the environment [26]. The polarization of an EM wave at the RX will change due to environmental changes just as the phase of the signal will change. Using two orthogonally-polarized antennas, a RX can measure both relative amplitudes and the phase between the two signals. Just like in (2), each polarized received signal has multipath component amplitudes and phases. These two measurements determine a point on a Poincaré sphere. The "differential polarization" can be determined by finding the angular change from an original polarization state to the current state. This differential can be calculated either with a time-average, or a frequency domain sub-band average. The latter is shown in [26] to provide a higher signal-to-noise ratio for detection of human-caused changes.

III. Models

All of the measurements described in Section II map changes in multipath components in order to locate and count the number of moving people (or objects) in the environment. Consider a person located at coordinate $\mathbf{x}_o$, and a link with TX location $\mathbf{x}_t$ and RX location $\mathbf{x}_r$, as depicted in Figures 1 and 2. In this section, we consider models for the relationship between changes caused to the multipath components by the person, and coordinate of the person, $\mathbf{x}_o$. Certainly, if changes are not a function of $\mathbf{x}_o$, we have no ability to locate the person. It is thus critical to have models to describe the changes in measurements as a function of position $\mathbf{x}_o$.

There are generally two views on the formulation of this position dependence.

1) *Relative position dependence*: The channel parameters are only a function of the relative position of $\mathbf{x}_o$ to TX and RX positions $\mathbf{x}_t$ and $\mathbf{x}_r$. For example, the parameters may only be a function of the distances $\|\mathbf{x}_o - \mathbf{x}_t\|$ and $\|\mathbf{x}_o - \mathbf{x}_r\|$. These assumptions are used in the algorithms presented in Sections IV-B through IV-H.
2) *Absolute position dependence*: The channel parameter dependence cannot be simplified using the relative positions of $\mathbf{x}_o$, $\mathbf{x}_t$, and $\mathbf{x}_r$ [1], [18], [17], [10].

In the latter case, the dependence of the measurement on $\mathbf{x}_o$ must be determined for every link (and thus $\mathbf{x}_t$ and $\mathbf{x}_r$), and for the entire range of $\mathbf{x}_o$, for each environment. Channel measurements are very sensitive to the placement and EM properties of all objects in the environment, and these positions and properties are highly likely to be unknown. Thus, measurements are required, at a high density of positions $\mathbf{x}_o$. For multiple people, the channel will have to be measured for all combinations of human locations. Algorithms which have this perspective are called fingerprint-based DFL, and are discussed in Section IV-A.

From the relative position dependence perspective, a statistical model describes the relationship between the channel changes experienced on a given link and $\mathbf{x}_o$, relative to $\mathbf{x}_t$ and $\mathbf{x}_r$. If knowledge about environmental objects is available (*e.g.*, wall locations) their relative positions w.r.t. $\mathbf{x}_t$ and $\mathbf{x}_r$ can also be used in the propagation model [27]. While not every link will experience the same changes given identical relative position information, if measured for many links, the distribution of changes should be characterized by the model. Such a statistical model could be generated from theory, or from many sets of measurements.

We do not suppose that a statistical model is accurate for all environments. True EM simulation or ray-tracing might be used if the properties, size, and position of objects in the environment were known. Or, perhaps these parameters can be considered "clutter" and measured so that a scatterer's position can be determined regardless [28], [29]. Statistical models are required when the complexity of typical static environments can not be accurately determined. Algorithms which do not make multipath propagation assumptions are discussed further in Section IV-B.

To formulate multipath channel models which provide position dependence, we primarily need to consider their spatial impact, rather than time delay and amplitude [25]. We denote $S_i(t)$ as the spatial filter of path i at time t. Generally, we model $S_i(t)$ as series of connected line segments, representing a plane wave changing direction at discrete points. Finally, to simplify the language, we simply refer to all objects which interact with a wave via transmission, diffraction, reflection, or

scattering, as "scatterers", regardless of the actual propagation mechanism.

A. Related Research

Fading models for static links dependent on the position of moving people are less prevalent than those for frequency-dependent fading or for space-dependent (small-scale) fading models. However, the reported literature has observations relevant to DFL, which we relate in this section.

In past studies, fading due to human motion was quantified to aid in the design of static communications systems which operate among moving people, *e.g.*, indoor WLANs [30], [31], [32], [33]. For indoor communications links, fading on a static link typically follows a Ricean mixture distribution, with a high variance when people are moving in and around the area of the link, and a low variance when they are not [30]. The Ricean K-factor depends on the power in "stationary" paths vs. power in "time-varying" paths due to motion [31]. Two-state Markov models have been used for simulation of static links, to account for this human-caused change in variance [32]. Researchers have observed that the motion of people near either the TX or RX impacts measured fading statistics, and in fact, when the number of people moving in proximity of TX or RX is increased, fading increases [33]. For example, the Rician K-factor decreases as the number of moving people in the area increases [34].

These general results show that human movement is measureable, and is generally a function of relative position and number of people. However, they do not provide a model for the fading as a function of the position of the moving people, with respect to the TX and RX coordinates.

B. Classification

Consider that at time t_0, a person did not exist in the environment, and that at time t_1, the person is located at position $\mathbf{x}_o$, as drawn in Figure 1. This section classifies multipath based on the changes to the multipath from time t_0 to time t_1.

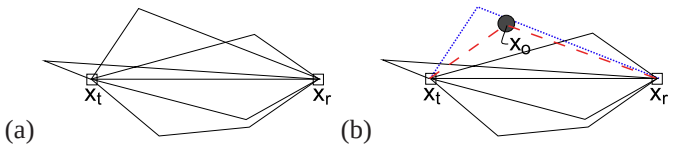

Fig. 1. (a) Example multipath components between TX at $\mathbf{x}_t$ and RX at $\mathbf{x}_r$. (b) When a person appears at $\mathbf{x}_o$, there are additional paths (- - - -) and alterations to existing multipath ($\cdots$).

The change in position of the person will affect some, but not all, of the amplitudes $\alpha_i(t)$ and time delays $\tau_i(t)$, and it will affect the number of multipath components $N(t)$. We classify the changes in the channel into three categories:

1) *Unaffected*: Some multipath components are unaffected. We denote the set of unaffected components as $\mathcal{T}_u$. For $i \in \mathcal{T}_u$, the path $S_i(t_0)$ does not intersect the person at $\mathbf{x}_o$.
2) *Affected*: Other multipath components change in amplitude and/or phase. We denote the set of affected components as $\mathcal{T}_a$. For $i \in \mathcal{T}_a$, $S_i(t_1)$ has altered to diffract around the person, or to transmit through the person, for example. We include the possibility that $|\alpha_i| \approx 0$ if the component is shadowed.
3) *New*: Some multipath components are created by the new person. In this case, $N(t_1)$ has increased, and we denote these new indices as $\mathcal{T}_n$. These new components are likely to be the result of scattering or reflecting from the new person.

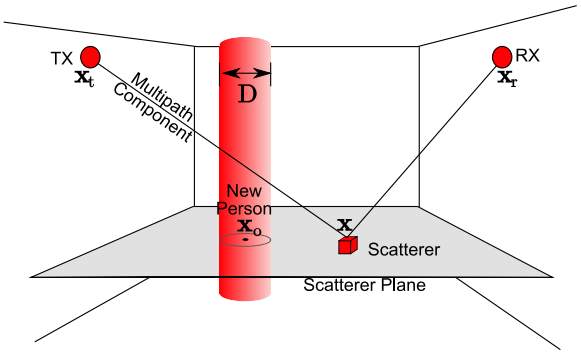

Fig. 2. TX, RX, plane containing scatterers, and the new person.

In the next two sections, we discuss the characteristics of new and affected multipath as a function of $\mathbf{x}_o$. First, in Section III-C, we discuss models for new multipath. Next, we discuss affected multipath in Section III-D.

C. New Multipath

Here, we discuss the new multipath created by the appearance of a person in the environment. It is typically assumed in the radar literature that an object appearing in the environment causes a new path from the TX to RX based on scattering from the object [35]. It is also assumed that this scatter-path is single-bounce, that is, the only change in direction in the path is due to the scattering. This model has appeared in indoor propagation models as well [36]. If $\mathbf{x}_o$ is the person location, the received power of the new scattered multipath is given by $P_s(\mathbf{x}_o)$, where

$$P_s(\mathbf{x}) = \frac{c_s}{\|\mathbf{x}_t - \mathbf{x}\|^2 \|\mathbf{x}_r - \mathbf{x}\|^2} \tag{4}$$

where c_s is a constant. The product of the squared distances in the denominator results from the scattering model, which says that the scatterer absorbs the incident power, and reradiates it in all directions, leading to a product of two Friis path loss equations.

We note that it is also possible that the new path is due to reflection. In this case, models such as [37] similarly assume a single-bounce path and state that the received power is given by $P_r(\mathbf{x}_o)$, where

$$P_r(\mathbf{x}) = \frac{c_r}{(\|\mathbf{x}_t - \mathbf{x}\| + \|\mathbf{x}_r - \mathbf{x}\|)^{n_p}} \tag{5}$$

where c_r is a constant, and n_p is the path loss exponent. Effectively, the only difference in received power compared to a line-of-sight path is due to the additional path length, and

perhaps a constant reflection loss contained within the constant c_r.

In the scattering case, the locus of points where $P_s(\mathbf{x}_o)$ is a constant is called a Cassini oval [35]. Cassini ovals are shown in Figure 3(a), which shows a contour plot of $P_s(\mathbf{x})$. In contrast, for reflection, the locus of points where $P_r(\mathbf{x}_o)$ is a constant is an ellipse. The lesson is that when the new multipath is caused by scattering, it has highest power when the person is near the TX or RX. But when the new path is from reflection, it has highest power when the person is anywhere in between the TX and RX.

D. Affected Multipath

In this section, we discuss models for the power in affected multipath as a function of the person's position. A multipath component is affected when its path crosses near the person at $\mathbf{x}_o$. For example, the component may diffract around the person, increasing the path length, thus changing its phase and increasing its time delay. An example geometry is shown in Figure 2, in which a person or object (with region of impact coarsely represented as a cylinder) will affect the multipath shown if either the line from the TX to scatterer, or from the scatterer to RX, cross through the person.

As mentioned in Section II-C, when measuring RSS variance, an important statistic is the total power in affected multipath,

$$P_a = \sum_{i \in \mathcal{T}_a} |V_i|^2 \tag{6}$$

This total power P_a varies depending on the particular environment (where scatterers are located). If we have a statistical model for the locations of scatterers and the propagation mechanism, we can derive a statistical model for P_a. For example, in [25], we use two indoor propagation models, [37] and [36], which model scatterer locations as a Poisson spatial process across a plane, and model multipath as a single-bounce phenomena. We apply these models to derive expressions for the ensemble mean of total affected power (ETAP), or $E[P_a]$. For the two cases where the mechanism of propagation is either all scattering or all reflection, Figures 3(b) and 3(c) show numerical results for P_a for an example link [25].

Compared to the power in new multipath, the spatial characteristics of reflection and scattering are reverse for power in affected multipath. For affected reflected multipath, the power is highest closest to the TX and RX, similar in shape to the Cassini oval, compared to new multipath power, which is highest in the line between the TX and RX. For affected scattered multipath, the power is highest near the line between the TX and RX, compared to new scattered multipath, which have highest power close to the TX and RX.

E. Measurement Verification

Since the theoretical models presented in the above sections require simplifying assumptions, it is critical to validate them via measurements. In this section, we present experimental evidence that has appeared in the literature.

As we mentioned in Section II-C, we have shown that the ensemble mean of total affected power, $E[P_a]$, has an approximately linear relationship with the ensemble mean of the variance of R_{dB} [25]. Thus we can use measurements of variance of R_{dB} in order to validate spatial models for $E[P_a]$.

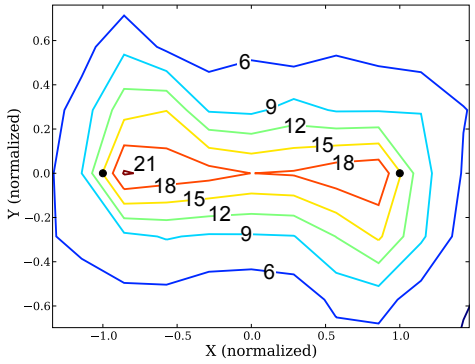

Fig. 4. Experimental RSS variance vs. $\mathbf{x}_o$ measured in a bookstore, normalized such that the RX (●) is located at (-1, 0) and the TX (●) is located at (1,0) [25].

Three measurement studies report the variance (or a related statistic) of R_{dB} as a function of $\mathbf{x}_o$ [24], [25], [8]. In two studies, measurements are conducted with RF sensors at body level in indoor environments with many scatterers, in an office [24], and in a bookstore [25]. In these studies, the variance of R_{dB}, and the "variation" (sum of absolute value of differences in a window of the time series) of R_{dB} are shown in Figures 4 and 5(a), respectively. Both results show highest changes in the areas nearest the TX and RX and next highest changes in the line between TX and RX. The third study performed a test in a building, but in an empty area, with RF sensors mounted on the ceiling, height 2.4 m [8]. This study found a different characteristic, that "dynamic" (average absolute value of the difference from the static mean) is highest in an oval centered at the midpoint of the line between the two nodes, as shown in Figure 5(b). It was shown in [25] that when the scattering plane is far separated from the RF sensor plane, the $E[P_a]$ surface becomes highest in the midpoint of the line between TX and RX, and falls with distance away from that point. Thus the results of [8] can be explained using analysis of affected multipath.

IV. Algorithms

Given that measurements of the channel are collected as described in Section II, and can be modelled as described in Section III, how should the positions of people in the environment be estimated? This is the inference problem discussed in this section. We present the algorithms studied in the literature, and provide a sample of the results obtained.

A. Fingerprint-based Methods

We describe in Section III the absolute position dependence perspective. From this perspective, localization is formulated as a fingerprint-matching problem [1], [18], [17], [10], [38] using a database of training measurements. During the online phase, the current state is estimated by comparison with

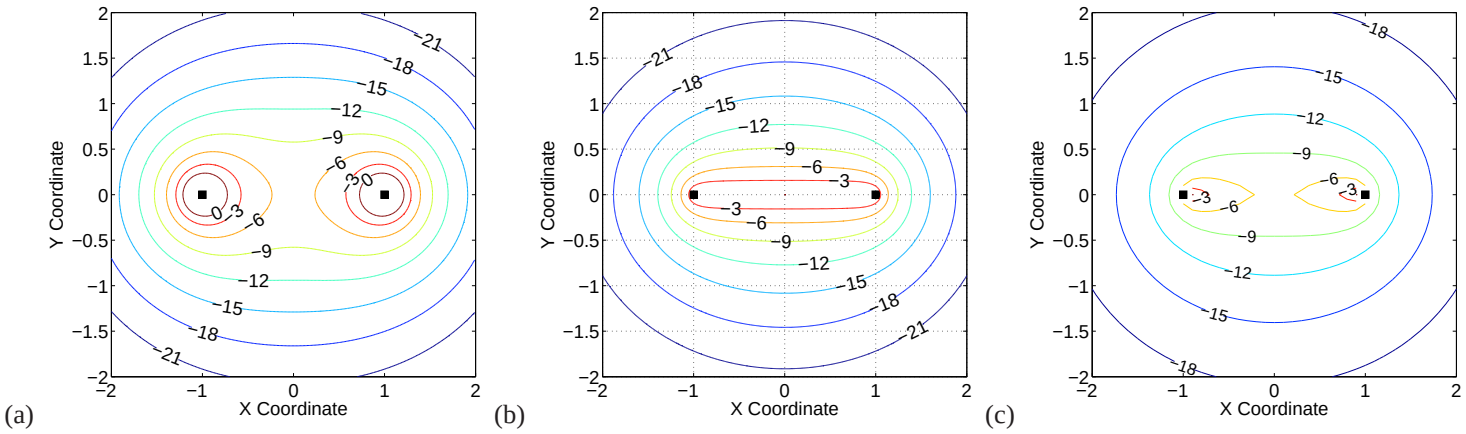

Fig. 3. (a) $P_s(\mathbf{x}_o)$ in dB relative to the maximum contour line; (b) and (c) ETAP in dB relative to the maximum [25] for (b) scattering, and (c) reflection (with $n_p = 3$). TX and RX locations are shown as ■.

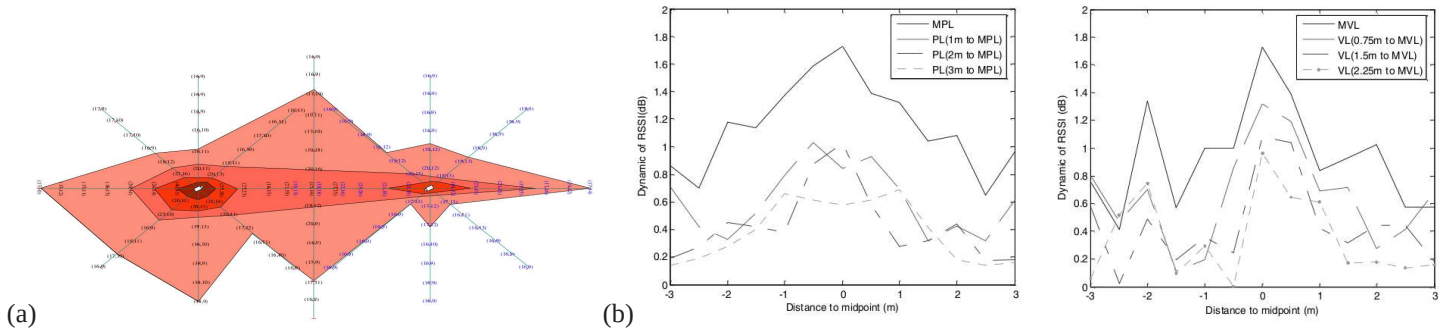

Fig. 5. Measured statistics as a function of $\mathbf{x}_o$ of (a) fading signal "variation" from [24], and (b) RSS "dynamic" for vertical line (VL) and parallel line (PL) slices, where MPL is the line between the TX and RX and MVL is perpendicular to MPL at its midpoint, which is labelled (0,0) [8].

Algorithm	**Measurement**	**Position Dependence**
Fingerprint-Matching [1], [17], [10]	RSS	Absolute
SVM [18], [38]	RSS	Absolute
Field Reconstruction [39]	Narrowband	Relative
Ultra-Narrowband [40], [41], [42], [43], [44]	Narrowband	Relative
MIMO Radar [45]	Narrowband or RSS	Relative
Geometric UWB [20], [35]	UWB	Relative
Probabilistic UWB [46], [47]	UWB	Relative
Mapping [48], [49]	UWB	Relative
Tomographic Imaging [50], [11], [15], [13]	RSS	Relative
Compressed Sensing [51], [52], [15]	RSS	Relative
Tracking from RSS [2], [13]	RSS	Relative
Motion Detection [16], [24]	RSS	n/a
Motion Detection [26]	Polarization	n/a
People Counting [9]	RSS	n/a

TABLE I
ALGORITHMS, MEASUREMENTS, AND POSITION DEPENDENCE.

the training measurements [1]. In [1], position estimates are found to be between 86% and 90% accurate. In [10], two distributions of RSS measurements for each link are found during training, one during motion in between the nodes, and one without any motion between the nodes. When a measurement is made during the online phase, a likelihood ratio test is done to determine which state was most likely. This is extended in [17] to measure an RSS histogram on each link for many possible positions of a person in a building area. Then, in the online phase, the maximum likelihood estimate (MLE) of the user's position is returned. A k-nearest neighbor "center of mass" technique is used to achieve a median error of 1.8 m. In [18], [38], the training data is used to train a support vector machine (SVM). Then, during the classification stage, the SVM classifier chooses the cell (small square area) from among all possible cells which is most likely to include the person based on the current RSS measurements.

A challenge in fingerprint-based algorithms is to track multiple people simultaneously, since training requirements increase exponentially with the number of people in the environment to be located, and to date, tests have only been done to track one person. Another challenge will be to self-correct the training data over time, to account for the changes in RSS histograms due to changes in the environment. For fingerprint-based real-time location service (RTLS) systems (locating radio tags), accuracy has been shown to degrade by up to 20% thirty days after training [53]. DFL systems are likely to be more sensitive to environmental changes than RTLS systems because they are in fact measuring what an RTLS system would consider an environmental change, that is, the position of a moving person. Finally, estimation of a histogram requires several measurements, for example 26 consecutive RSS measurements in [17], or 60 seconds in [1], while a person is standing in one location. In a real-time system, RSS data would need to be

collected more quickly in order to track a person in motion.

B. EM Wave Field Reconstruction

Estimation of the spatio-temporal EM wave field in an environment of interest is a possibility when narrowband measurements (of $\tilde{V}$) are performed. If an object affects the spatio-temporal EM wave field, then its location and track can be seen in this estimate. Electromagnetic wave propagation equations can be solved using the measurement of complex baseband voltage around two concentric perimeters around the area of interest [39]. Then, the wave equations can be approximated using the conjoint cylindrical wave expansion. Phase-synchronous measurements of $\tilde{V}$ are made by moving a single antenna to each measurement position.

A similar approach [40], [41], [42], [43] is called "ultra-narrowband (UNB) radar", in contrast to UWB, because of its transmission and reception of a CW signal rather than a wideband signal. UNB uses phase-coherent measurements at locations surrounding a target and Fourier-based tomographic reconstruction to image scattering as a function of space. For example, in [43], measurements are made by placing an object on a rotating table to simulate what would happen if sensors were placed every two degrees around the object. In theory, a few phase-synchronous transceivers can be used to create a "virtual tomographic array" which can reposition the phase center of the transmitted signal to points in the convex hull of the transceivers [44] which then reduce the need for phase synchronous transceivers.

The term *microwave subsurface tomography* is used generally to refer to methods which image the radar cross-section (RCS) of objects behind or below a surface [54], [55] using phase-coherent measurements of the EM wave field. These methods model the field as described by Green's function, the electric field measured due to a line current induced on the scattering object [54], [28], [56]. Sensor measurements can be expressed as a Fourier transform of the field of interest [54], [55]. However, it is assumed that sensors form an antenna array, or equivalently, sensors are phase-synchronous. Measurement experiments typically use a single transmitter and receiver automatically moved between antenna locations [55].

C. MIMO Radar

Multiple transmit waveforms, transmit antennas, and receive antennas can be used in combination to improve radar detection and imaging performance. Because these radar methods are similar to MIMO communications systems, the area is termed *MIMO radar*. MIMO radar with non-coherent receivers and widely separated antennas enables a type of spatial diversity that is useful for DFL. The backscatter from a complex object (an object which scatters from more than one point) is a function of angle, so multiple receivers at different angles lead to more reliable detection [45]. Transmitters in a MIMO radar system use orthogonal waveforms so that they can be separated at the receivers. These orthogonal waveforms may result from time-division multiplexing (as is typically used in most DFL research), frequency-division multiplexing, or some other orthogonal basis.

The challenge in application of MIMO radar techniques to DFL in building environments is to account for cluttered multipath channels. MIMO radar research generally considers only the additional scattering caused by an object, that is, $\mathcal{T}_a$ is assumed to be empty. In remote sensing and airplane radar systems, this assumption is reasonable, but DFL systems operate in a rich multipath environment in which an object disrupts or blocks other multipath. However, meeting this challenge is important to gain the ability to image static features of an environment, which is a benefit of the MIMO radar framework.

D. UWB Tracking and Data Association

In contrast to narrowband measurements, UWB impulse response measurements allow separation of multipath changes as a function of time delay. Chang and Sahai explored DFL using a network of single or multiple UWB receivers in addition to single or multiple UWB transmitters [20]. The authors assume that the changes in the CIR are only those from new multipath, and consider cases when $\mathbf{x}_o$ is either inside, or outside, of the hull of the sensor network. The Cramér-Rao lower bound (CRLB) is derived and asymptotics presented for the case when nodes are uniformly spaced on a circle of radius R centered at the origin. The CRLB work assumes one object in the field, and that the channel impulse response can be used to pick out the delay of the impulse corresponding to that sole object. The estimated delay is unbiased and Gaussian, and based on the single-bounce model. They showed that for N transmitters and M receivers, the Fisher information for the object location was $\mathcal{O}\left(\frac{1}{NM}\right)$, and that for the far-field case, was $\mathcal{O}\left(\|\mathbf{x}_o\|^2/R^2\right)$. Chang and Sahai presented a "semi-linear" object localization algorithm, which is sub-optimal but has performance which behaves similarly to the lower bound as a function of N and $\mathbf{x}_o$. For the case of multiple people, the authors discuss the data association problem, in which each delay must be associated with exactly one of the people.

Work by Paolini et. al. [35] further investigates the capabilities of the system described in [20]. Importantly, the authors describe the geometry of the area of detection of a UWB link based on amplitude and time delay. When the new multipath scattered power $P_s(\mathbf{x}_o)$ falls below a threshold, the system can no longer effectively identify its time delay. Thus $\mathbf{x}_o$ must be within a Cassini oval with foci $\mathbf{x}_t$ and $\mathbf{x}_r$, as described in Section III-C, to be detectable. Further, the temporal resolution limits of the impulse response estimate prevent a scatterer from being detected if it is very close to the line of sight path. Thus there is a narrow ellipse with foci at the TX and RX location in which resolution prevents TOA estimation.

Work in [46] advanced the field by considering that each person introduces not just one new multipath component, but several, in a cluster of time delays with the single-bounce path being the shortest. Second, it is not trivial to select the new multipath impulse from the measured CIR, which prior to the person's entry already contained many paths. Reggiani et. al. [46] compared 'hard' thresholding and 'soft' probabilistic quantification in multinode UWB tracking systems. They

also showed a method to adaptively quantify the variance of a distance estimate. This ranging data from multiple nodes is used for multi-target tracking using an extended Kalman filter (EKF) bank. They show, using CIRs obtained from ray-tracing simulations, that the location accuracy improves when using soft information and variance estimates. The EKF bank benefits significantly from redundancy – more filters than scatterers, which is beneficial "since tracking more distance combinations helps to recover all the useful cluster arrivals in the dense received impulse responses" [46].

The work of Rydström et. al. shows the importance, in multiple target tracking, of properly formulating data association [47]. In this case, data association is the problem of assigning each distance measurement to one object being tracked. While Chang and Sahai presented an intuitively appealing 'score' function [20] for purposes of data association, the method of [47] is based on a weighted least-squares (WLS) cost function and a Lagrangian relaxation technique for its optimization. In general, the complexity of the data association problem is exponential in the number of measurements. However, impossible assignments can be quickly pruned [47]. Further, the Lagrangian relaxation algorithm is based on an auction algorithm which can be solved in polynomial time, thus the assignment problem can be framed in computationally feasible manner. Simulations show that the data association approach outperforms the score function of [20].

Finally, Rydström et. al. note that the accuracy of passive localization approaches the accuracy possible from active localization, assuming the same system and device parameters. That is, placing an UWB tag on a person or object allows for better localization, compared to localization of the device-free person or object, but not by a large margin. While use of a tag provides identification in addition to localization, we should not ignore the capabilities of device-free localization, when identification or tagging is not needed or possible.

Note the above UWB-based methods do not assume synchronization. However, they do assume known node positions and that a LOS path exists. Without synchronization, the time-of-arrival of the LOS path is used to determine the excess time delays corresponding to the scatterers. A challenge for DFL based on UWB will be to be robust to the case when the LOS TOA cannot be obtained.

E. Mapping

An advantage of UWB measurements is that they contain information about the static environment, in addition to information about the mobile people and objects. Simulation-based work in [48] presents the capabilities of an UWB radar to simultaneously track its own movement over time, and estimate a map of the walls of a room, based on delays $\tau(t)$ from measured CIRs measured over time t. An algorithm which accepts unlabeled delays must first decide from which wall (or which combinations of walls) that path reflected. Then, it may estimate the dimensions and the angles at the corners of the room. Such mapping has been demonstrated using a set of static UWB TXs and a single mobile UWB RX in a cluttered industrial environment [49].

F. Imaging

One approach to DFL is to estimate an image of the change in environment. This image can then be used to infer the motion and activity within the environment, either by a human operator, or by an image processing algorithm.

Image estimation from measurements along different spatial filters through a medium is generally referred to as tomographic image reconstruction. For RF sensors, this is termed radio tomographic imaging (RTI) [50], [11], [15], [13]. A network of N static sensors measures up to $\binom{N}{2}$ "slices" through the medium. Let the measurements on all links be vector $\mathbf{y} = [y(1), \ldots, y(L)]^T$, where L is the number of measured links. Then, let the vector of voxel values be $\mathbf{x} = [x(1), \ldots, x(P)]^T$, where P is the number of voxels. A linear model for $\mathbf{y}$ may be written as,

$$\mathbf{y} = A\mathbf{x} + \mathbf{n}$$

where A is an $L \times P$ matrix, and $\mathbf{n}$ is additive noise. RTI is the estimation of image $\mathbf{x}$ from measurements $\mathbf{y}$.

In [11], $\mathbf{y}$ is the change in R_{dB} from the historical value on each link, and it is modelled as linear combination of the $\mathbf{x}$, the attenuation in dB caused by each voxel in the environment. This model is called shadowing-based RTI, since the measurements effectively measure shadowing loss, and the image estimates are shown to accurately display the location one or two people in the deployment area [11]. The linear model for shadowing loss is based on correlated shadowing models [57], [50] and earlier linear partition-loss models [58].

Another modality of RTI is termed variance-based RTI, in which the windowed variance of R_{dB} on each link is used as the measurement $\mathbf{y}$, and $\mathbf{x}$ represents a quantification of the motion within each voxel [13]. This linear model for variance has basis in the results described in Section III-D, in which the presence of motion at $\mathbf{x}_o$ causes a certain quantity of multipath power to be affected, and the measured variance of R_{dB} on a link is approximately linearly related to the total affected power.

Experimental tests reported in [13] show that variance-based RTI can image the motion going on inside a house, when sensors are placed only outside of its external walls, as shown in Figure 6(a). In the case of imaging motion through building walls, we can have the problem that the multipath which travel around the building can be stronger than the power in paths which travelled through the building. Analytical results in [13] suggest that the change in variance can be detected even when the power in the affected multipath is 10 dB less than the multipath which do not go through the building.

However, tomography is generally an ill-posed problem, and regularization is required to reduce the noise in the image and to achieve "smoothness" or other intuitively desireable image properties. In [12], three methods of regularization, Tikanov, truncated singular value decomposition (TSVD), and total variation (TV) are applied. Tikanov regularization is both computationally simple, robust to noise and model mismatch. Image estimation using Tikanov regularization is a linear transform of data $\mathbf{y}$, and thus is simply a matrix multiplication. Tikanov and TV regularization are compared in Figure 6(b)

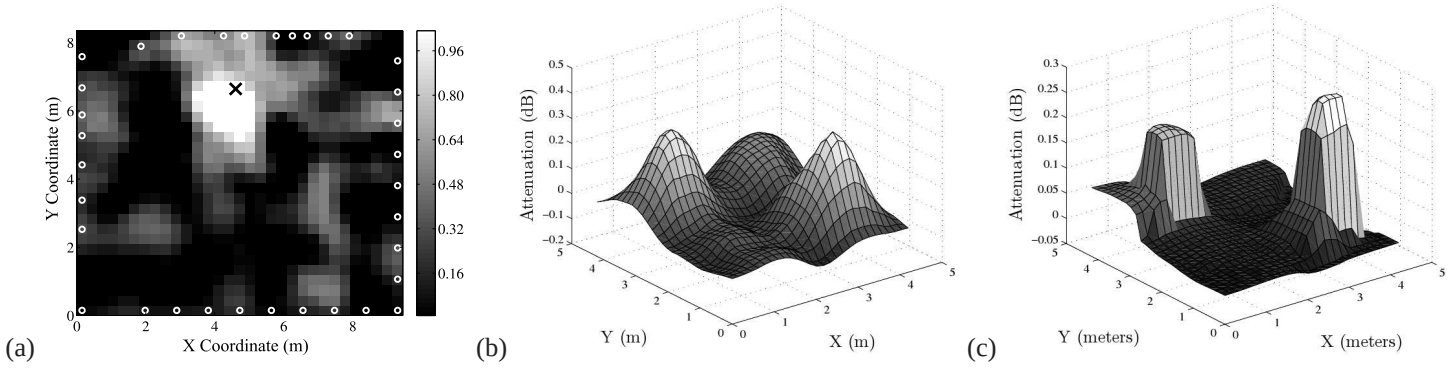

Fig. 6. Image estimates for (a) through-building variance-based RTI when a moving person is located at the × [13], and mean-based RTI with (b) Tikanov and (c) total variation regularization, with two people in the area [12].

and (c). TV regularization can produce sharp images with well-defined edges, but require numerical optimization, which is more computationally intensive than Tikanov regularization.

G. Compressed Sensing

Kanso and Rabbat have investigated an alternative to regularization, *i.e.*, a "compressed sensing" (CS) approach to radio tomographic imaging [51], [52], [15]. First, the image can be estimated using a constrained l_1 minimization [52]. Secondly, the image can be obtained using the LASSO technique [59], and thirdly, using orthogonal matching pursuit (OMP) [60] [15]. The latter approaches find image estimate $\hat{\mathbf{x}}$ by solving,

$$\hat{\mathbf{x}} = \underset{\mathbf{x}}{\operatorname{argmin}} \ \|A\mathbf{x} - \mathbf{y}\|_2^2 + \lambda\|\mathbf{x}\|_1, \tag{7}$$

where λ is a tunable parameter, and $\|\cdot\|_1$ and $\|\cdot\|_2$ indicate vector l_1 and l_2 norm, respectively. One benefit of the approach is that image estimates $\hat{\mathbf{x}}$ have sharp contrast, with very few pixels containing non-zero values. Secondly, imaging requires fewer links, and thus can require less probing energy to be expended. Even when only 25% of links are measured, the detection and imaging performance is nearly the same as with all links [51]. Finally, the minimization of (7) can be distributed on the sensors, using a projection on convex sets (POCS) method, which converges quickly [15]. Such distributed algorithms will be important for the deployment of large-scale DFL systems, so that measured data does not need to be collected at a central location for processing.

The challenge in application of CS to DFL is to provide sparse images even with the high noise level contained in RF tomographic measurements. Currently, the number of pixels should be set low in order to improve tracking performance with experimental data [51].

H. Tracking from RSS

A step beyond localization is tracking, *i.e.*, the estimation of both position and velocity (and perhaps higher order derivatives of position) over a period of time. The first DFL system using RSS measurements was proposed by Woyach, Puccinneli, and Haenggi, who coined the term "sensorless sensing" to describe cases when the radio itself is the sensor [2]. One sensorless sensor system presented measures RSS on multiple stationary links across a hallway. Using the changes in each link RSS, crossing is inferred, which is used to estimate the track and velocity of a person walking through the hallway.

Image estimates can be used as an input for tracking algorithms. For example, the maximum of an image is a coordinate which can be tracked using a Kalman filter [13]. An experiment reported in [13] used images using variance-based RTI as an input to imaging algorithms. The peak of the image is input to a Kalman filter to track the location of person inside of a home with an average error of 0.5 and 1 m in two experiments.

Zhang et. al. present an algorithm which directly estimates a human's track from link measurements [8]. For each link which measures RSS variation above a threshold, the area in which the person is likely to be located is approximated as a rectangle, centered at the midpoint of the line between TX and RX. Then a "best-cover algorithm" estimates the person's position, which is input into a tracking filter Experiments show tracking error as low as 1 m. This work was extended in [14] to use a clustering algorithm for multi-object tracking.

I. Motion Density Estimation

Sometimes, only the presence of a person, or the number of people in an area, is of importance for an application. For this purpose, we can use RSS fading measurements on a link. Nakatsuka, Iwatani, and Katto [9] experimentally derive linear relationships between the RSS mean and variance (or LQI) and the number of people walking or sitting between two nodes, for use in crowd density estimation. Their results show that a linear relationship exists for a 4.5 m link between the number of people (up to nine) and both the fading variance and change in mean. For a longer 8.0 m link, the linear relationship holds even up to 20 people, although there are saturation effects in some experiments.

A similar experimental setup in [16] is used to test whether or not a person is walking from one node to the other. Experiments are conducted in a variety of different indoor and outdoor environments. The authors show that the differences between subsequent R_{dB} values have a consistent distribution in both cases (motion or no motion), regardless of environment. This consistency can enable more robust detection of motion.

V. Research Directions

Considerable future work exists if DFL is to be deployed for the applications mentioned in the Introduction. We mention a few open problems here. First, are single-bounce models acceptable for DFL in indoor environments? They may be too simplistic in complicated environments. Future work must test multiple-bounce models to determine if they can provide increased levels of accuracy. Electromagnetic characteristics of the objects strongly affect the propagation in the environment. Can more complicated electromagnetic models be applied without prior knowledge of environmental characteristics?

Second, tracking and adaptation are important topics. Propagation models may be adapted based on past measurements, in order to learn the geometric paths of multipath components and their amplitudes. In addition, multi-target tracking must be applied to the cases when measurements are narrowband or RSS-only. What are good and robust means to separate the multipath changes made by each person in a large-scale RF sensor network? Related to the adaptation question, do training measurements with one person in the environment allow the determination of what would be measured when multiple people exist in the environment?

Device-free localization requires that measurements are frequent enough to measure during the event of a person or object moving through the links of the network. For human motion, measurements might be on the order of one per second, and for vehicle motion, measurements will need to be made more often. Further, a measurement requires both a transmitter and receiver to be on (not in a sleep state). What tradeoffs exist between energy consumption and localization accuracy? What practical algorithms can be used to duty cycle sensors, or to process data locally so that uninformative measurements do not need to be forwarded?

Finally, in localization systems which track moving people and objects who wear active tags, can device-free localization be used to improve the accuracy of active location estimates, and if so, at what cost? Finally, if RF sensor networks are to be deployed in larger numbers, across entire buildings or facilities, how will the data be processed, using a central processor, or distributed among the sensors? In either case, sensor networking protocols must be designed for the critical low-latency requirements of the applications.

VI. Conclusion

An emerging application of wireless sensor networking is the use of networks of RF sensors for device-free localization. In this application, static sensors use radio channel measurements to infer the presence and position of people and objects moving in the environment of deployment. Unlike sensor localization or RTLS, people do not carry a radio tag, and instead are located based on the changes they cause to the channels between static RF sensors. We review measurements which can be made in multistatic RF sensor networks to be used for DFL. We discuss models which relate the statistics of these measurements, as a function of the position of the person. Finally, we review algorithms which have been applied for DFL. Results from published literature include: average location errors lower than 1 meter using only measurements of signal strength; the number of moving people, up to 20, can be estimated from a single link; the movements of multiple people can be tracked using UWB measurements, or imaged using RF tomography.

References

[1] M. Youssef, M. Mah, and A. Agrawala, "Challenges: device-free passive localization for wireless environments," in *MobiCom '07: ACM Int'l Conf. Mobile Computing and Networking*, pp. 222–229, 2007.

[2] K. Woyach, D. Puccinelli, and M. Haenggi, "Sensorless sensing in wireless networks: Implementation and measurements," in *WiNMee 2006*, April 2006.

[3] R. R. Rogers and W. O. J. Brown, "Radar observations of a major industrial fire," *Bulletin of the Amer. Meteorological Soc.*, vol. 78, pp. 803–814, May 1997.

[4] P. Bahl and V. N. Padmanabhan, "RADAR: an in-building RF-based user location and tracking system," in *IEEE INFOCOM 2000*, vol. 2, pp. 775–784, 2000.

[5] H. Hashemi, "The indoor radio propagation channel," *Proc. IEEE*, vol. 81, pp. 943–968, July 1993.

[6] K. Pahlavan, P. Krishnamurthy, and J. Beneat, "Wideband radio propagation modeling for indoor geolocation applications," *IEEE Comm. Magazine*, vol. 36, pp. 60–65, April 1998.

[7] W. A. Kalender, *Computed Tomography: Fundamentals, System Technology, Image Quality, Applications*. Wiley, 2006.

[8] D. Zhang, J. Ma, Q. Chen, and L. M. Ni, "An RF-based system for tracking transceiver-free objects," in *IEEE PerCom'07*, pp. 135–144, 2007.

[9] M. Nakatsuka, H. Iwatani, and J. Katto, "A study on passive crowd density estimation using wireless sensors," in *The 4th Intl. Conf. on Mobile Computing and Ubiquitous Networking (ICMU 2008)*, June 2008.

[10] M. Moussa and M. Youssef, "Smart services for smart environments: Device-free passive detection in real environments," in *IEEE PerCom-09*, pp. 1–6, 2009.

[11] J. Wilson and N. Patwari, "Radio tomographic imaging with wireless networks," *IEEE Trans. Mobile Computing*, 2009. (accepted).

[12] J. Wilson and N. Patwari, "Regularization methods for radio tomographic imaging," in *2009 Virginia Tech Symposium on Wireless Personal Communications*, June 2009.

[13] J. Wilson and N. Patwari, "Through-wall motion tracking using variance-based radio tomography networks," Tech. Rep. arXiv:0909.5417v2, arXiv.org, Oct. 2009. Available at http://arxiv.org/abs/0909.5417.

[14] D. Zhang, J. Ma, Q. Chen, and L. M. Ni, "Dynamic clustering for tracking multiple transceiver-free objects," in *IEEE PerCom'09*, pp. 1–8, 2009.

[15] M. A. Kanso and M. G. Rabbat, "Compressed RF tomography for wireless sensor networks: Centralized and decentralized approaches," in *5th IEEE Intl. Conf. on Distributed Computing in Sensor Systems (DCOSS-09)*, (Marina Del Rey, CA), June 2009.

[16] P. W. Lee, W. K. Seah, H. Tan, and Z. Yao, "Wireless sensing without sensors – an experimental approach," in *PIMRC-09*, Sept. 2009.

[17] M. Seifeldin and M. Youssef, "Nuzzer: A large-scale device-free passive localization system for wireless environments," Tech. Rep. arXiv:0908.0893, Arxiv.org, Aug. 2009.

[18] F. Viani, L. Lizzi, P. Rocca, M. Benedetti, M. Donelli, and A. Massa, "Object tracking through RSSI measurements in wireless sensor networks," *IEE Electronics Letters*, vol. 44, no. 10, pp. 653–654, 2008.

[19] N. Patwari, A. O. Hero III, M. Perkins, N. Correal, and R. J. O'Dea, "Relative location estimation in wireless sensor networks," *IEEE Trans. Signal Process.*, vol. 51, pp. 2137–2148, Aug. 2003.

[20] C. Chang and A. Sahai, "Object tracking in a 2D UWB sensor network," in *38th Asilomar Conference on Signals, Systems and Computers*, vol. 1, pp. 1252–1256, Nov. 2004.

[21] A. Lin and H. Ling, "Three-dimensional tracking of humans using very low-complexity radar," *Electronics Letters*, vol. 42, pp. 1062–1063, 31 2006.

[22] F. Sivrikaya and B. Yener, "Time synchronization in sensor networks: a survey," *IEEE Network*, vol. 18, pp. 45–50, July-Aug. 2004.

[23] M. Maroti, B. Kusy, G. Balogh, P. Volgyesi, K. Molnar, A. Nadas, S. Dora, and A. Ledeczi, "Radio interferometric positioning," Tech. Rep. ISIS-05-602, Institute for Software Integrated Systems, Vanderbilt University, Nov. 2005.

[24] Q. Yao, H. Gao, B. Liu, and F. Wang, "MODEL: moving object detection and localization in wireless networks based on small-scale fading," in *ACM SenSys'08)*, pp. 451–452, 2008.
[25] N. Patwari and J. Wilson, "People-sensing spatial characteristics of RF sensor networks," Tech. Rep. arXiv:0911.1972v1, arXiv.org, Nov. 2009. Available at http://arxiv.org/abs/0911.1972.
[26] T. Pratt, S. Nguyen, and B. Walkenhorst, "Dual-polarized architectures for sensing with wireless communications signals," in *IEEE MILCOM 2008*, pp. 1–6, 2008.
[27] E. J. Baranoski, "Through-wall imaging: Historical perspective and future directions," *Journal of the Franklin Institute*, vol. 345, no. 6, pp. 556–569, 2008.
[28] L. Li, W. Zhang, and F. Li, "A novel autofocusing approach for real-time through-wall imaging under unknown wall characteristics," *Geoscience and Remote Sensing, IEEE Transactions on*, vol. 48, pp. 423 –431, Jan 2010.
[29] J. Moura and Y. Jin, "Time reversal imaging by adaptive interference canceling," *IEEE Transactions on Signal Processing*, vol. 56, no. 1, pp. 233–247, 2008.
[30] R. J. Bultitude, "Measurement, characterization, and modeling of indoor 800/900 MHz radio channels for digital communications," *IEEE Communications*, vol. 25, no. 6, pp. 5–12, 1987.
[31] T. S. Rappaport and C. D. McGillem, "UHF fading in factories," *IEEE Journal on Sel. Areas in Comm.*, vol. 7, pp. 40–48, Jan. 1989.
[32] J. A. Roberts and J. R. Abeysinghe, "A two-state Rician model for predicting indoor wireless communication performance," in *IEEE ICC*, vol. 1, pp. 40–43, June 1995.
[33] H. Hashemi, "A study of temporal and spatial variations of the indoor radio propagation channel," in *PIMRC-94*, vol. 1, pp. 127–134, Sep 1994.
[34] K. I. Ziri-Castro, N. E. Evans, and W. G. Scanlon, "Propagation modelling and measurements in a populated indoor environment at 5.2 GHz," in *2006 Auswireless Conference*, 2006.
[35] E. Paolini, A. Giorgetti, M. Chiani, R. Minutolo, and M. Montanari, "Localization capability of cooperative anti-intruder radar systems," *EURASIP Journal on Advances in Signal Processing*, pp. 1–14, 2008. Article ID 236791.
[36] O. Nørklit and J. B. Andersen, "Diffuse channel model and experimental results for array antennas in mobile environments," *IEEE Trans. Antennas & Propagation*, vol. 46, pp. 834–840, June 1998.
[37] J. C. Liberti and T. S. Rappaport, "A geometrically based model for line-of-sight multipath radio channels," in *IEEE 46th Vehicular Technology Conference*, vol. 2, pp. 844–848, 1996.
[38] F. Viani, P. Rocca, M. Benedetti, G. Oliveri, and A. Massa, "Electromagnetic passive localization and tracking of moving targets in a WSN-infrastructured environment," *Inverse Problems*, vol. 26, pp. 1–15, March 2010.
[39] R. Pirkl and G. Durgin, "Quasi 2-D field reconstruction using the conjoint cylindrical wave expansion," *IEEE Transactions on Antennas and Propagation*, vol. 57, no. 4, pp. 1095–1104, 2009.
[40] M. C. Wicks, B. Himed, L. J. E. Bracken, H. Bascom, and J. Clancy, "Ultra narrow band adaptive tomographic radar," in *1st IEEE Intl. Workshop Computational Advances in Multi-Sensor Adaptive Processing*, Dec. 2005.
[41] M. Wicks, B. Himed, H. Bascom, and J. Clancy, "Tomography of moving targets (TMT) for security and surveillance," *NATO Advanced Study Institute Advances in Sensing with Security Applications, Il Ciocco, Italy*, pp. 323–339, 2006.
[42] H. D. Griffiths and C. J. Baker, "Radar imaging for combatting terrorism," in *NATO Advanced Study Institute Imaging for Detection and Identification*, pp. 1–19, July/August 2006.
[43] S. L. Coetzee, C. J. Baker, and H. Griffiths, "Narrow band high resolution radar imaging," in *IEEE Conf. on Radar*, pp. 24–27, April 2006.
[44] K. Magde and M. Wicks, "Waveforms in virtual tomographic arrays," in *Intl. Waveform Diversity and Design Conf.*, pp. 83–87, 2007.
[45] A. M. Haimovich, R. S. Blum, and L. J. Cimini, "MIMO radar with widely separated antennas," *IEEE Signal Processing*, vol. 25, pp. 116–129, Jan. 2008.
[46] L. Reggiani, M. Rydström, G. Tiberi, E. G. Ström, and A. Monorchio, "Ultra-wide band sensor networks for tracking point scatterers or relays," in *Sixth International Symposium on Wireless Communication Systems 2009 (ISWCS-09)*, Sept. 2009.
[47] M. Rydström, E. G. Ström, A. Svensson, and L. Reggiani, "An algorithm for positioning relays and point scatterers in wireless systems," *IEEE Signal Processing Letters*, vol. 15, pp. 381–384, 2008.
[48] W. Guo, N. P. Filer, and R. Zetik, "Indoor mapping and positioning using impulse radios," in *2006 IEEE/ION Position, Location, And Navigation Symposium (PLANS-06)*, pp. 153–163, 2006.
[49] R. Thomä, O. Hirsch, J. Sachs, and R. Zetik, "UWB sensor networks for position location and imaging of objects and environments," in *Antennas and Propagation, 2007. EuCAP 2007. The Second European Conference on*, pp. 1–9, 2007.
[50] N. Patwari and P. Agrawal, "Effects of correlated shadowing: Connectivity, localization, and RF tomography," in *IEEE/ACM Int'l Conf. on Information Processing in Sensor Networks (IPSN'08)*, pp. 82–93, April 2008.
[51] M. A. Kanso, "Compressed RF tomography: Centralized and decentralized methods," Master's thesis, McGill University, 2009.
[52] M. A. Kanso and M. G. Rabbat, "Efficient detection and localization of assets in emergency situations," in *3rd Intl. Symposium on Medical Information & Communication Technology (ISMICT)*, (Montréal, Québec), Feb. 2009.
[53] K. W. Kolodziej and J. Hjelm, *Local positioning systems: LBS applications and services*. CRC Press, Taylor & Francis Group, 2006.
[54] L. Chommeloux, C. Pichot, and J.-C. Bolomey, "Electromagnetic modeling for microwave imaging of cylindrical buried inhomogeneities," *IEEE Transactions on Microwave Theory and Techniques*, vol. 34, pp. 1064–1076, Oct. 1986.
[55] A. A. Vertiy and S. P. Gavrilov, "Subsurface tomography application for through-wall imaging," in *Proc. 9th International Conference on Electromagnetics in Advanced Applications (ICEAA-05) and 11th European Electromagnetic Structures Conference (EESC-05)*, pp. 12–16, 2005.
[56] D. Liu, G. Kang, L. Li, Y. Chen, S. Vasudevan, W. Joines, Q. Liu, J. Krolik, and L. Carin, "Electromagnetic time-reversal imaging of a target in a cluttered environment," *IEEE Transactions on Antennas and Propagation*, vol. 53, no. 9, pp. 3058–3066, 2005.
[57] P. Agrawal and N. Patwari, "Correlated link shadow fading in multi-hop wireless networks," *IEEE Trans. Wireless Commun.*, vol. 8, pp. 4024–4036, Aug. 2009.
[58] G. D. Durgin, T. S. Rappaport, and H. Xu, "Measurements and models for radio path loss and penetration loss in and around homes and trees at 5.85 GHz," *IEEE Trans. Communications*, vol. 46, pp. 1484–1496, Nov. 1998.
[59] R. Tibshirani, "Regression shrinkage and selection via the lasso," *Journal of the Royal Statistical Society. Series B (Methodological)*, vol. 58, no. 1, pp. 267–288, 1996.
[60] J. Tropp and A. Gilbert, "Signal recovery from random measurements via orthogonal matching pursuit," *IEEE Transactions on Information Theory*, vol. 53, pp. 4655–4666, Dec. 2007.